Mon. Not. R. Astron. Soc. **385,** 2243–2253 (2008) doi:10.1111/j.1365-2966.2008.12996.x

Gamma-ray probe of cosmic ray pressure in galaxy clusters and cosmological implications

Shin'ichiro Ando★ and Daisuke Nagai★
California Institute of Technology, Mail Code 130-33, Pasadena, CA 91125, USA

Accepted 2008 January 19. Received 2007 December 19; in original form 2007 May 16

ABSTRACT

Cosmic rays produced in cluster accretion and merger shocks provide pressure to the intracluster medium (ICM) and affect the mass estimates of galaxy clusters. Although direct evidence for cosmic ray ions in the ICM is still lacking, they produce γ-ray emission through the decay of neutral pions produced in their collisions with ICM nucleons. We investigate the capability of the *Gamma-ray Large Area Space Telescope* (*GLAST*) and imaging atmospheric Čerenkov telescopes (IACTs) for constraining the cosmic ray pressure contribution to the ICM. We show that *GLAST* can be used to place stringent upper limits, a few per cent for individual nearby rich clusters, on the ratio of pressures of the cosmic rays and thermal gas. We further show that it is possible to place tight ($\lesssim$10 per cent) constraints for distant ($z \lesssim 0.25$) clusters in the case of hard spectrum, by stacking signals from samples of known clusters. The *GLAST* limits could be made more precise with the constraint on the cosmic ray spectrum potentially provided by IACTs. Future γ-ray observations of clusters can constrain the evolution of cosmic ray energy density, which would have important implications for cosmological tests with upcoming X-ray and Sunyaev–Zel'dovich effect cluster surveys.

Key words: radiation mechanisms: non-thermal – cosmic rays – galaxies: clusters: general – cosmology: miscellaneous – gamma-rays: theory.

1 INTRODUCTION

Clusters of galaxies are potentially powerful observational probes of dark energy, the largest energy budget in the Universe causing the cosmic acceleration (e.g. Haiman, Mohr & Holder 2001; Albrecht et al. 2006). Most of the cosmological applications using clusters rely on the estimates of their total virial mass – quantity which is difficult to measure accurately in observations. Clusters offer a rich variety of observable properties, such as X-ray luminosity and temperature (e.g. Rosati, Borgani & Norman 2002), Sunyaev–Zel'dovich effect (SZE) flux (e.g. Carlstrom, Holder & Reese 2002), gravitational lensing of distant background galaxies (e.g. Smith et al. 2005; Bradač et al. 2006; Dahle 2006) and velocity dispersion of cluster galaxies (e.g. Becker et al. 2007) and proxies for cluster mass.

One of the most widely used methods for measuring cluster masses relies on the assumption of hydrostatic equilibrium between gravitational forces and thermal pressure gradients in the intracluster medium (ICM) (Sarazin 1986; Evrard, Metzler & Navarro 1996). Current X-ray and SZE observations can yield mass of individual clusters very precisely based on accurate measurements of the density and temperature profiles (Pointecouteau, Arnaud & Pratt 2005; LaRoque et al. 2006; Vikhlinin et al. 2006). However, the accuracy of the hydrostatic mass estimates is currently limited by non-thermal pressure provided by cosmic rays, turbulence and magnetic field in the ICM (Enßlin et al. 1997; Rasia et al. 2006; Nagai, Vikhlinin & Kravtsov 2007a, and references therein). This non-thermal bias must be understood and quantified before the requisite mass measurement accuracy is achieved. Comparisons with the mass estimates from gravitational lensing can provide potentially useful limits on this non-thermal bias (see e.g. Mahdavi et al. 2007). However, present observations do not yet constrain the non-thermal pressure in the regime in which it dramatically affects the calibration of the hydrostatic mass estimates. If not accounted for, these non-thermal biases limit the effectiveness of upcoming X-ray and SZE cluster surveys to accurately measure the expansion history of the Universe. Detailed investigations of sources of non-thermal pressure in clusters are thus critical for using clusters of galaxies as precision cosmological probes.

There is growing observational evidence for the non-thermal activity in clusters. For example, radio and hard X-ray observations of clusters suggest presence of relativistic electrons. This also implies presence of relativistic protons produced in the shock that accelerated these electrons. However, the signature γ-ray emission due to decays of neutral pions produced in the collisions of cosmic rays with nucleons in the ICM has not been detected. From non-detection of γ-ray emission from clusters with the *Energetic Gamma Ray Experimental Telescope* (*EGRET*) in the GeV band (Reimer et al. 2003; but see also Kawasaki & Totani 2002; Scharf & Mukherjee 2002), constraints have been placed on the fraction of cosmic ray

★E-mail: ando@caltech.edu; daisuke@caltech.edu

© 2008 The Authors. Journal compilation © 2008 RAS

pressure in nearby rich clusters at less than ∼20 per cent (Enßlin et al. 1997; Miniati 2003, Virgo and Perseus clusters) and less than ∼30 per cent (Pfrommer & Enßlin 2004, Coma cluster). Similar constraints are obtained using the Whipple Čerenkov telescope in the TeV band (Perkins et al. 2006). In addition, indirect constraints can be obtained from radio observations (e.g. Brunetti et al. 2007). These measurements indicate that the cosmic rays provide relatively minor contribution to the dynamical support in the ICM (e.g. Blasi 1999). However, the current constraints are too loose for the future cluster-based cosmological tests.

The next generation of γ-ray detectors, such as *Gamma-ray Large Area Space Telescope* (*GLAST*) and imaging atmospheric Čerenkov telescopes (IACTs), will be able to provide dramatically improved constraints on the cosmic ray pressure in clusters, and may even detect γ-ray radiation from several rich clusters (Ando et al. 2007a, and references therein). The *GLAST* satellite, which is soon to be launched, is equipped with the Large Area Telescope (LAT) that enables all sky survey with GeV γ-rays. Several IACTs are currently working or planned for detecting TeV γ-rays, which include H.E.S.S., MAGIC, VERITAS and CANGAROO-III. Confronting the recent advances in γ-ray astronomy as well as growing interests in dark energy studies, in the present paper, we investigate the sensitivity of these detectors to high-energy γ-rays of cosmic ray origin.

We first show updated sensitivities of *GLAST* and IACTs for nearby rich clusters following Pfrommer & Enßlin (2004). In particular, *GLAST* would be able to constrain the cosmic ray energy density in such clusters to better than *a few per cent* of the thermal energy density, while IACTs would be useful to constrain the cosmic ray spectrum. We then consider stacking many γ-ray images of distant clusters to probe the evolution of cosmic ray pressure. We show that, by stacking many massive clusters, the upcoming *GLAST* measurements will have the statistical power to constrain the cosmic ray pressure component to better than ∼10 per cent of the thermal component for clusters out to $z \lesssim 0.25$. These forthcoming measurements will be able to place stringent limits on the bias in the cluster mass estimates and hence provide important handle on systematic uncertainties in cosmological constraints from upcoming X-ray and SZE cluster surveys.

Throughout this paper, we adopt the concordance cosmological model with cold dark matter and dark energy (ΛCDM), and use $\Omega_{\rm m} = 0.3, \Omega_\Lambda = 0.7, H_0 = 100\,h\,{\rm km\,s^{-1}\,Mpc^{-1}}$ with $h = 0.7$ and $\sigma_8 = 0.8$.

2 GAMMA-RAY PRODUCTION DUE TO PROTON–PROTON COLLISIONS

Cosmic ray protons are injected in the ICM through the shock wave acceleration, and the momentum distribution follows the power law, $p_{\rm p}^{-\alpha_{\rm p}}$ with $\alpha_{\rm p} \simeq 2$–3. These cosmic ray protons then interact with the surrounding ICM (mostly non-relativistic protons), producing neutral and charged pions; the former decays into two photons ($\pi^0 \to 2\gamma$) while the latter into electrons, positrons and neutrinos. The volume emissivity of the π^0-decay γ-rays (number per volume per unit energy range) at distance r from the cluster centre is given as (e.g. Blasi & Colafrancesco 1999)

$$q_\gamma(E, r) = 2n_{\rm H}(r)c \int_{E_{\pi,\rm min}}^{\infty} {\rm d}E_\pi \int_{E_{\rm p,th}(E_\pi)}^{\infty} {\rm d}E_{\rm p} \times \frac{{\rm d}\sigma_{\rm pp}}{{\rm d}E_\pi}(E_\pi, E_{\rm p}) \frac{n_{\rm p}(E_{\rm p}, r)}{\sqrt{E_\pi^2 - m_\pi^2 c^4}}, \quad (1)$$

where m_π and E_π is the mass and energy of the neutral pion, $E_{\pi,\rm min} = E + m_\pi^2/4E$ is the minimum pion energy required to produce a photon of energy E, and similarly $E_{\rm p,th}(E_\pi)$ is the minimum energy of protons for pion production. The density of ICM, $n_{\rm H}(r)$, is very well measured by the X-ray observations of bremsstrahlung radiation from thermal electrons, and the cross-section of the proton–proton collision for pion production, ${\rm d}\sigma_{\rm pp}/{\rm d}E_\pi$, can be calibrated using laboratory data. The distribution function of cosmic ray protons $n_{\rm p}(E_{\rm p}, r)$ depends on the injection power, spectrum and spatial distribution of cosmic rays. By specifying these ingredients, we can predict the γ-ray flux from a cluster.

In practice, we use a fitting formula as well as cluster parameters given in Pfrommer & Enßlin (2004); for the former, we briefly summarize it in Appendix A. In addition, one should also note that electrons and positrons produced by $\pi^\pm$ decays can scatter cosmic microwave background (CMB) photons up to γ-ray energies. For a while, we neglect this secondary process, but revisit it in Section 6 and show that it is in fact negligible under most of realistic situations.

2.1 Cosmic ray power and spectrum

The cosmic ray pressure $P_{\rm p}$ and energy density $\rho_{\rm p}$, which are the quantities that we want to constrain, are directly related to the injection power of the cosmic rays. The cosmic ray spectrum is measured to be a power law with the index of $\alpha_{\rm p} = 2.7$ in our Galaxy, but in the clusters it is perhaps harder, since they can confine cosmic rays for cosmological times (Völk, Aharonian & Breitschwerdt 1996; Berezinsky, Blasi & Ptuskin 1997; Enßlin et al. 1997). We thus adopt harder spectrum with $\alpha_{\rm p} = 2.1$ and 2.4, but also use $\alpha_{\rm p} = 2.7$ as a limiting case.

It is also possible that the injection of the cosmic rays and thus their energy density $\rho_{\rm p}$ are intermittent. Although it is interesting to constrain the source property by measuring such γ-ray variability, this is not the primary focus in the present paper. Instead, we concentrate on constraining energy density $\rho_{\rm p}$ averaged over *GLAST* exposure time. For the sensitivity of *GLAST*, we consider the result of one-year all-sky survey, which corresponds to ∼70-d exposure to each source as the field of view is ∼20 per cent of the whole sky. Therefore, any time variability within this 70-d duration is smeared out.

2.2 Radial distribution

We define quantities $X_{\rm p}$ and $Y_{\rm p}$ as ratios of energy density and pressure of cosmic rays to those of thermal gas, respectively, i.e.

$$X_{\rm p} \equiv \frac{\rho_{\rm p}}{\rho_{\rm th}}, \quad Y_{\rm p} \equiv \frac{P_{\rm p}}{P_{\rm th}}. \quad (2)$$

In general, these depend on the radius, but the concrete dependence is totally unknown. Various mechanisms supplying the cosmic ray protons have been proposed, which produce characteristic and diverse profiles of $X_{\rm p}$ and $Y_{\rm p}$. We thus parametrize them using a simple power law

$$X_{\rm p}(r) = X_{\rm p}(R_{500}) \left(\frac{r}{R_{500}}\right)^\beta,$$
$$Y_{\rm p}(r) = Y_{\rm p}(R_{500}) \left(\frac{r}{R_{500}}\right)^\beta, \quad (3)$$

where R_Δ (here $\Delta = 500$) is the radius at which the enclosed spherical overdensity is Δ times the critical density of the Universe at the

cluster's redshift,[1] where the cluster mass M_Δ is traditionally defined with the X-ray and SZE measurements. We note that this approach ignores boosts in γ-ray flux caused by clumpiness. The constraints derived using a smooth model hence provide a conservative upper limit on X_p and Y_p.

We first focus on X_p, and later discuss Y_p. The relation between γ-ray intensity and X_p is summarized in Appendix A and that between X_p and Y_p is discussed in Section 5. We shall study the dependence of results on β, for which we adopt 1, 0 and -0.5. Below, we outline several models that motivate these values of β.

2.2.1 *Isobaric model*

The simplest model is based on the assumption of $\beta = 0$, i.e. the energy density of cosmic rays precisely traces that of thermal gas everywhere in the cluster. The latter is proportional to temperature times number density of the thermal gas, both of which are very well measured with X-rays for various nearby clusters. The gas density profile is nearly constant within a characteristic core radius r_c, beyond which it decreases as a power law, while temperature profile is almost constant. The core radius and outer profile are $r_c = 300$ kpc, $r^{-2.3}$ (Coma), $r_c = 200$ kpc, $r^{-1.7}$ (Perseus) and $r_c = 20$ kpc, $r^{-1.4}$ (Virgo) (see table 1 of Pfrommer & Enßlin 2004, for a more comprehensive list). The latter two clusters have an even smaller 'cool core', but this structure gives only a minor effect on the γ-ray flux.

2.2.2 *Large-scale structure shocks*

The formation of galaxy clusters is due to merging or accretion of smaller objects. When this occurs, the shock waves are generated at the outskirts of the clusters, somewhere around ~3 Mpc from the centre, where protons and electrons are accelerated to relativistic energies (e.g. Loeb & Waxman 2000; Miniati 2002; Gabici & Blasi 2003; Keshet et al. 2003). Unlike electrons that immediately lose energies through synchrotron radiation and inverse Compton (IC) scattering off CMB photons, protons are hard to lose energies, and they are transported efficiently into the cluster centre following the motion of ICM gas (Miniati et al. 2001). In order to predict the eventual profile of the cosmic ray energy density, one needs to resort to numerical simulations. The recent radiative simulations by Pfrommer et al. (2007) show somewhat jagged shape for the $X_p(r)$ profile, which implies large clumping factor. Here, we model its global structure with a smooth profile with $\beta = -0.5$, ignoring the effects of clumpiness. On the other hand, they also performed non-radiative simulations which rather imply $\beta = 1$ profile. Although the latter may not be realistic, the effects of cooling and heating in clusters are also somewhat uncertain. Thus, we still adopt this model, treating it as an extreme case.

2.2.3 *Central point source*

A central powerful source such as active galactic nuclei or cD galaxy might be an efficient supplier of the cosmic rays, which diffuse out from the central region after injection. The profile of cosmic ray energy density is r^{-1}, but truncated at a radius that is far smaller than R_{500} for relevant energies (Berezinsky et al. 1997; Colafrancesco & Blasi 1998). The actual γ-ray detection might therefore cause significant overestimate of the cosmic ray pressure; we address this issue in Section 3.2.

Numerical simulations of jets from active galactic nuclei suggest that temporal intermittency and spatial structure might be complicated (e.g. O'Neill et al. 2005). Neither of these, however, affects our results that depend on global and time-averaged properties.

3 COSMIC RAY ENERGY DENSITY IN NEARBY GALAXY CLUSTERS

3.1 Constraints from entire region of clusters

We first discuss the case of the Coma cluster, focusing on the region within $R_{500} = 2.1$ Mpc and assuming the isobaric distribution of the cosmic ray energy density ($\beta = 0$). Fig. 1 shows the integrated γ-ray flux with photon energies above $E_{\rm min}$, $F(>E_{\rm min})$, for $X_p = 0.1$. This flux is to be compared with the sensitivities of *GLAST* and IACTs, for which one has to take the source extension into account. Indeed, the radial extension of the Coma cluster R_{500} corresponds to $\theta_{500} = 1^\circ.2$, which at high energies exceeds the size of the point spread function (PSF), $\delta\theta_{\rm PSF}(E)$. We obtain the flux sensitivity for an extended source from that for a point source by multiplying a factor of max $[1, \theta_{500}/\delta\theta_{\rm PSF}(E_{\rm min})]$, if the sensitivity is limited by backgrounds. On the other hand, if the expected background count from the cluster region is smaller than 1, which is the case for *GLAST* above ~30 GeV, the sensitivities for a point source and an extended source are identical. The region ~2–30 GeV is where the expected background count is smaller than 1 from the PSF area but larger than 1 from the entire cluster. We assume that IACTs are limited by background over the entire energy region, and we multiply the point-source sensitivity by $\theta_{500}/\delta\theta_{\rm PSF}$ with $\delta\theta_{\rm PSF} = 0^\circ.1$; this is consistent with Aharonian et al. (1997) for relevant energy

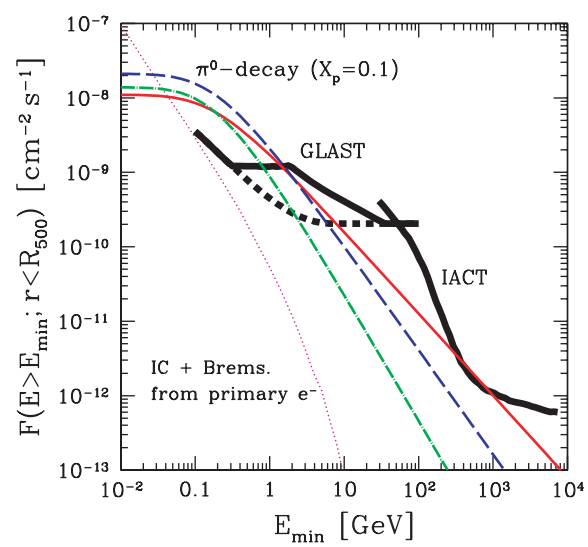

Figure 1. Flux of γ-ray emission from the region within $R_{500} = 2.1$ Mpc of the Coma cluster, for the isobaric model with $X_p = 0.1$ (labelled as 'π^0 decay'). The spectral index of the cosmic ray protons is $\alpha_p = 2.1$ (solid), 2.4 (dashed) and 2.7 (dot–dashed). The sensitivity curves of *GLAST* and IACTs are for a source extended by $\theta_{500} = 1^\circ.2$ (corresponding to R_{500}), while the point-source sensitivity of *GLAST* is also shown as a short dashed curve. Flux due to IC scattering and non-thermal bremsstrahlung is also shown (dotted; from Reimer et al. 2004).

[1] We use $R_\Delta hE(z) = r_5(T_{\rm spec}/5\,{\rm keV})^{\eta/3}$, where $r_5 = 0.792\,h^{-1}$ Mpc and $\eta = 1.58$ for $\Delta = 500$, $r_5 = 0.351\,h^{-1}$ Mpc and $\eta = 1.64$ for $\Delta = 2500$ and $E^2(z) = \Omega_{\rm m}(1+z)^3 + \Omega_\Lambda$ for the flat ΛCDM cosmology (Vikhlinin et al. 2006).

Table 1. Sensitivity to $X_p(R_{500})$ of *GLAST* ($E_{min} = 100$ MeV) for various values of spectral index of cosmic rays α_p, and isobaric and large-scale structure shock models for radial distribution or β. The limits on X_p are set by the γ-ray flux from a region within whichever of the larger between the PSF $\delta\theta_{PSF}(E_{min}) \approx 3^\circ$ and the source extension θ_{500}.

		$X_{p,lim}(R_{500})$ for $\beta = 1$			$X_{p,lim}(R_{500})$ for $\beta = 0$			$X_{p,lim}(R_{500})$ for $\beta = -0.5$		
Cluster	θ_{500}	$\alpha_p = 2.1$	$\alpha_p = 2.4$	$\alpha_p = 2.7$	$\alpha_p = 2.1$	$\alpha_p = 2.4$	$\alpha_p = 2.7$	$\alpha_p = 2.1$	$\alpha_p = 2.4$	$\alpha_p = 2.7$
Coma	1°.2	0.11	0.063	0.10	0.040	0.022	0.035	0.018	0.0098	0.016
Perseus	1°.5	0.024	0.013	0.022	0.012	0.0068	0.011	0.0050	0.0027	0.0044
Virgo	4°.6	0.076	0.042	0.067	0.041	0.022	0.036	0.016	0.0088	0.014
Ophiuchus	1°.3	0.088	0.048	0.078	0.020	0.011	0.018	0.0064	0.0035	0.0056
Abell 2319	0°.6	0.048	0.027	0.043	0.057	0.031	0.050	0.032	0.018	0.029

regime. A more detailed derivation of this sensitivity is given in Appendix C.

We also show flux of IC scattering and bremsstrahlung radiations from electrons primarily accelerated in the shocks (Reimer et al. 2004). The authors suggested that these electron components would always be below the *GLAST* and IACT sensitivities, based on constraints from radio, extreme ultraviolet (EUV), and hard X-ray observations. If this is the case, the γ-ray detection would imply existence of cosmic ray protons, and be used to constrain the pressure from this component (see also, Enßlin, Lieu & Biermann 1999; Atoyan & Völk 2001). We give more detailed discussions about IC mechanisms in Section 6.

Fig. 1 shows that γ-rays from π^0 decays are detectable for $X_p = 0.1$. In particular, the models with different values of α_p predict similar amount of γ-ray fluxes for low-energy thresholds ($E_{min} < 1$ GeV); *GLAST* measurements can therefore provide constraints on X_p, almost independent of α_p. Non-detection with *GLAST* from these nearby clusters is also very interesting as it provides very tight upper limit to the cosmic ray energy density in clusters. The fluxes above ~1 TeV, on the other hand, depends very sensitively on α_p; IACTs will thus constrain the spectral index.

In Table 1, we summarize the sensitivity to $X_p(R_{500})$ for *GLAST* in the case of $E_{min} = 100$ MeV, for several values of α_p and different models of radial distribution of cosmic ray energy density. We also performed the same analysis for other nearby rich clusters (Perseus, Virgo, Ophiuchus and Abell 2319), and report their results as well. This indeed confirms that the *GLAST* constraints on X_p depend only weakly on the assumed spectral index.[2] The constraints improve for smaller values of β. For $\beta \leqslant 0$, the *GLAST* non-observation can place tight upper limits on the cosmic ray energy density at a few per cent level. Even in the case of non-radiative large-scale structure shock model ($\beta = 1$) the constraint is still as good as ~10 per cent for the Coma. This is a dramatic improvement from the *EGRET* bounds (see e.g. table 3 of Pfrommer & Enßlin 2004), by more than an order of magnitude.

On the other hand, the IACT constraints on X_p (with $E_{min} =$ 1 TeV) for the Coma cluster and $\beta = 0$ profile are 0.37, 2.3 and 42 for $\alpha_p = 2.1$, 2.4 and 2.7, respectively. Thus, IACTs will therefore provide constraints on the spectral index, which is directly related to astrophysical mechanisms of particle acceleration. A similar trend can be found in table 6 of Pfrommer & Enßlin (2004); however, the authors applied point-source flux limit to the (extended) clusters and obtained much more stringent sensitivities than ours.

[2] Note that the sensitivity peaks at $\alpha_p = 2.5$. This is because for even larger α_p, the contribution from low-momentum protons to the energy density becomes more significant, while they do not produce γ-rays.

3.2 Direct constraint from large radii

So far, we treated all clusters but Virgo as point sources. Although we showed that the dependence on the assumed radial profile was reasonably weak, a more general approach would be to use the resolved image. This is particularly useful, if the radial profile cannot be simply parametrized (see Section 2.2). Because we are interested in the cosmic ray pressure at R_{500} and the γ-ray yields would rapidly drop with radius, we here consider constraints in a projected radial shell between θ_{2500} and θ_{500}. We mainly focus on the Perseus, and assume $\alpha_p = 2.1$; in this case, $\theta_{2500} = 0°.65$. In order to resolve the inner region, we consider the energy threshold of 0.6 GeV, above which the *GLAST* resolution becomes smaller than θ_{2500}. The *GLAST* flux limits for the outer region and for $E > 0.6$ GeV correspond to the following limits on the fractional energy density: $X_{p,lim}(R_{500}) = 0.099$, 0.089 and 0.080, for $\beta = 1$, 0 and -0.5, respectively, which are still reasonably small. In addition, these are much less sensitive to the assumed profile, thus applicable to more general cases including the central source model. The similar procedure predicts sensitivities for other clusters: $X_p(R_{500}) = 0.42$ (Coma), 0.14 (Virgo), 0.41 (Ophiuchus) and 0.55 (Abell 2319), in the case of $\beta = 0$ and $\alpha_p =$ 2.1. Although it is limited to nearby clusters, such analysis provides an important handle on the radial distribution of cosmic ray ions in clusters.

4 EVOLUTION OF COSMIC RAY ENERGY DENSITY

While we could obtain stringent constraints for individual nearby clusters, these rapidly get weaker for more distant clusters. In this case, however, one can stack many clusters to overcome the loss of signals from each cluster. Reimer et al. (2003) took this approach for the *EGRET* analysis, and obtained an improved upper limit to the average flux of 50 nearby clusters. We argue that the flux is not a physical quantity because it depends on distance and therefore distribution of sources. We should instead convert this improved flux limit to constraint on more physical quantities such as γ-ray luminosity. Here, we examine the *GLAST* constraints on $X_p(R_{500})$ obtained by stacking clusters from the whole sky and in several redshift intervals. As we consider rather distant clusters, they are all treated as point sources.

4.1 Stacking γ-ray signals from galaxy clusters

4.1.1 Formulation and models

The number of clusters with $M > M_{th}$ between redshifts z_1 and z_2 is given by

$$N_{cl} = \int_{z_1}^{z_2} dz \frac{dV}{dz} \int_{M_{th}}^{\infty} dM \frac{dn_h}{dM}(M, z), \quad (4)$$

where $\mathrm{d}V$ is the comoving volume element, $\mathrm{d}n_\mathrm{h}/\mathrm{d}M$ is the halo mass function (comoving number density of dark matter haloes per unit mass range); the former can be computed given cosmological parameters, and for the latter we use the following parametrization:

$$\frac{\mathrm{d}n_\mathrm{h}}{\mathrm{d}M_\mathrm{180m}} = A_\mathrm{J}\frac{\Omega_\mathrm{m}\rho_\mathrm{c}}{M_\mathrm{180m}}\exp\left(-\left|\ln\sigma^{-1}+B_\mathrm{J}\right|^{\epsilon_\mathrm{J}}\right)\frac{\mathrm{d}\ln\sigma^{-1}}{\mathrm{d}M_\mathrm{180m}}, \tag{5}$$

where ρ_c is the critical density of the present Universe, σ (M_180m, z) is a standard deviation for distribution function of linear over density, $A_\mathrm{J} = 0.315, B_\mathrm{J} = 0.61$ and $\epsilon_\mathrm{J} = 3.8$ (Jenkins et al. 2001). Here we note that M_180m is defined as an enclosed mass within a given radius, in which the average density is $180\Omega_\mathrm{m}\rho_\mathrm{c}(1+z)^3$.

We give the threshold mass $M_\mathrm{th}(z)$ in terms of threshold temperature T_th based on the observed mass–temperature relation: $M_{200} = 10^{15}\,h^{-1}\,\mathrm{M}_\odot\,(T/8.2\,\mathrm{keV})^{3/2}\,E(z)^{-1}$ (Voit 2005). This is because the efficiency of large-scale SZE cluster surveys relies mainly on cluster temperature *regardless of* cluster redshifts. Note that this relation is between temperature and mass M_{200}, which is within a radius R_{200}. Here we use the prescription of Hu & Kravtsov (2003) for the conversion of different mass definitions, M_{200} and M_180m with assumed concentration parameter $c_\mathrm{v} = 3$. For the threshold temperature, we adopt $T_\mathrm{th} = 3$ and 5 keV. Fig. 2(a) shows the mass function as well as threshold mass corresponding to T_th, at various redshifts. In Table 2, we list values of N_cl after integrating equation (4), for several redshift ranges and different T_th.

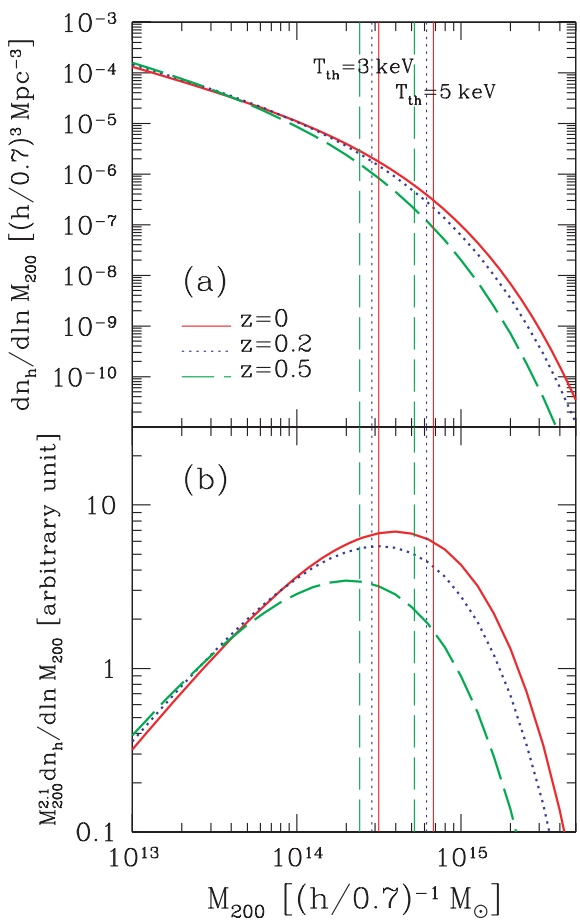

Figure 2. (a) Cluster mass function as a function of M_{200} at several redshifts. Threshold mass M_th corresponding to $T_\mathrm{th} = 3$, 5 keV is shown as vertical lines. (b) Cluster mass function $\mathrm{d}\,n_\mathrm{h}/\mathrm{d}\ln M_{200}$ multiplied by $M_{200}^{2.1}(\propto F_{X_\mathrm{p}})$, in arbitrary units. Line types are the same as in (a).

Table 2. *GLAST* sensitivities to $X_\mathrm{p}(R_{500})$ and $Y_\mathrm{p}(R_{500})$ by stacking N_cl clusters above threshold temperature T_th at given redshift ranges, for $\alpha_\mathrm{p} = 2.1, \beta = 0$ and $E_\mathrm{min} = 1$ GeV.

	$T_\mathrm{th} = 3$ keV			$T_\mathrm{th} = 5$ keV		
z	N_cl	$X_\mathrm{p,lim}$	$Y_\mathrm{p,lim}$	N_cl	$X_\mathrm{p,lim}$	$Y_\mathrm{p,lim}$
0.05–0.10	200	0.11	0.06	30	0.09	0.05
0.10–0.15	530	0.21	0.11	60	0.16	0.09
0.15–0.25	2500	0.29	0.16	290	0.23	0.13
0.25–0.40	7900	0.57	0.31	870	0.46	0.25
0.40–0.60	17000	1.3	0.72	1700	1.1	0.60

The average flux of γ-rays from these clusters is

$$\overline{F}_{\mathrm{st},X_\mathrm{p}} = \frac{1}{N_\mathrm{cl}}\int_{z_1}^{z_2}\mathrm{d}z\frac{\mathrm{d}V}{\mathrm{d}z}\int_{M_\mathrm{th}}^{\infty}\mathrm{d}M\frac{\mathrm{d}n_\mathrm{h}}{\mathrm{d}M}(M,z)F_{X_\mathrm{p}}(M,z), \tag{6}$$

where $F_{X_\mathrm{p}}(M,z)$ is the γ-ray flux from a cluster of mass M at redshift z, given X_p. The flux from each cluster above E_min is written as

$$F_{X_\mathrm{p}}(M,z) = \frac{1+z}{4\pi d_\mathrm{L}^2}\int\mathrm{d}V_\mathrm{cl}\int_{(1+z)E_\mathrm{min}}^{\infty}\mathrm{d}E\;q_\gamma(E,r\,|\,M), \tag{7}$$

where d_L is the luminosity distance, $\mathrm{d}V_\mathrm{cl}$ represents the cluster volume integral, and q_γ is the volume emissivity given by equation (1) or (A1).

We then quantify the mass dependence of this flux $F_{X_\mathrm{p}}(M,z)$. In the case of the isobaric model ($\beta = 0$) with a fixed X_p, the γ-ray luminosity scales as ICM number density times energy density, i.e. $L_\gamma \propto X_\mathrm{p}n_\mathrm{H}\rho_\mathrm{th} \propto X_\mathrm{p}n_\mathrm{H}^2T$. On the other hand, luminosity of X-rays due to the thermal bremsstrahlung process scales as $L_\mathrm{X} \propto n_\mathrm{H}^2T^{1/2}$. Therefore, there is a relation between γ-ray and X-ray luminosities as follows: $L_\gamma/L_\mathrm{X} \propto X_\mathrm{p}T^{1/2}$. In addition, there are empirical relations between X-ray luminosity and cluster mass, $L_\mathrm{X} \propto M_{200}^{1.8}$, and also between gas temperature and mass, $T \propto M_{200}^{2/3}E^{2/3}(z)$ (Voit 2005). Thus, combining these three and assuming that X_p is independent of mass, we obtain a scaling relation $L_\gamma \propto X_\mathrm{p}M_{200}^{2.1}\,E^{1/3}(z)$. In Fig. 3, we show predicted γ-ray luminosity as a function of cluster mass (inferred from temperature), for several well-measured nearby clusters (taken from tables in Pfrommer & Enßlin 2004) with the parameters $X_\mathrm{p} = 0.1, \alpha_\mathrm{p} = 2.1$ and $\beta = 0$. The L_γ–M_{200} relation can indeed be well fitted with $L_\gamma(>100\,\mathrm{MeV}) = 7.6\times10^{44}\,X_\mathrm{p}(M_{200}/10^{15}\,h^{-1}\,\mathrm{M}_\odot)^{2.1}$ erg s^{-1} for clusters at $z \approx 0$, shown as a solid line in Fig. 3. When we compute the γ-ray flux $F_{X_\mathrm{p}}(M\,|\,z)$ (or equivalently luminosity) from clusters with a given mass M, we adopt this mass–luminosity relation as a model for average cluster, and scale as $L_\gamma \propto E^{1/3}(z)$ for high-redshift clusters.

Fig. 2(b) shows the mass function weighed by the mass dependence of the flux (in arbitrary unit). This quantity represents which mass scale dominates the average flux at each redshift. From this figure, one can see that clusters with $M_{200} \sim 3\times10^{14}\,\mathrm{M}_\odot$ most effectively radiates γ-rays in the low-redshift universe, but the distribution is rather broad for $\sim10^{14}$–$10^{15}\,\mathrm{M}_\odot$. If we adopt $T_\mathrm{th} = 5$ keV, then the clusters around the threshold mass are the more dominant contributors to the average flux.

4.1.2 GLAST constraints on X_p

The average flux of the stacked clusters (equation 6) is then compared with the corresponding *GLAST* sensitivity,

$$F_\mathrm{st,lim} = \frac{F_\mathrm{lim}}{\sqrt{N_\mathrm{cl}}}, \tag{8}$$

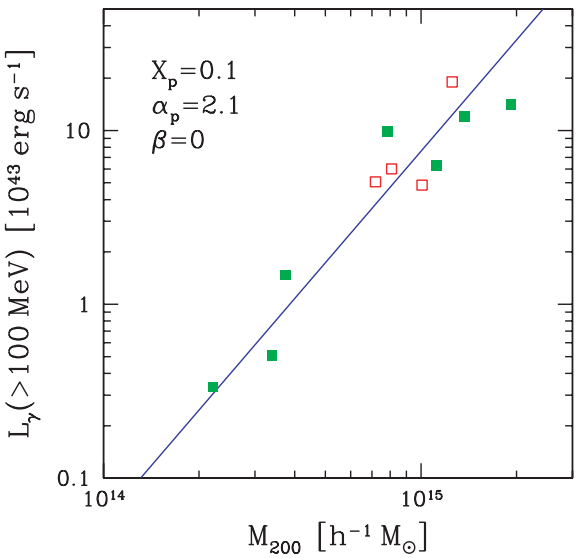

Figure 3. Relation between γ-ray luminosity (above 100 MeV) and cluster mass M_{200}, for several nearby clusters and for the parameters $X_p = 0.1$, $\alpha_p = 2.1$ and $\beta = 0$. Filled (open) points are for cooling flow (non-cooling flow) clusters. The solid line is the $L_\gamma \propto M_{200}^{2.1}$ profile that fits the data quite well.

where $F_{\rm lim}$ is the sensitivity to each cluster given as the thick dashed line in Fig. 1 (for a point-like source). To derive constraints on X_p from the stacked image, we solve $\overline{F}_{{\rm st},X_p} = F_{\rm st,lim}$ for X_p. Throughout the following discussion, we adopt $\beta = 0$, $\alpha_p = 2.1$ and $E_{\rm min} = 1$ GeV, around which the γ-ray yields are maximized compared with the point-source sensitivity (Fig. 1). In addition, the pixel number with this threshold (4 π divided by PSF area; 6×10^4) is large enough to minimize the positional coincidence of multiple clusters (compare with $N_{\rm cl}$ values in Table 2).

We summarize the results in Table 2. We find that the limits are as strong as $X_p \lesssim 0.16$ (0.23) for $0.1 < z < 0.15$ ($0.15 < z < 0.25$). The sensitivities improve for larger $T_{\rm th}$, because the smaller cluster number is compensated by the strong mass dependence of the flux. The constraints on X_p degrades rapidly with redshift. Table 2 also shows *GLAST* sensitivities for Y_p, which is almost twice as stringent as those for X_p in the case of $\alpha_p = 2.1$. We discuss implications of this result for Y_p in Section 5 in details.

The current X-ray catalogue covers clusters at $z \lesssim 0.2$ for $T_{\rm th} = 5$ keV (Böhringer et al. 2001). The *GLAST* data could thus immediately be compared with this low-redshift catalogue. At higher redshifts, the South Pole Telescope would find many clusters with $T \gtrsim 3$ keV using SZE; but since it covers ~10 per cent of the whole sky, the limits would become around three times weaker than those in Table 2. The *Planck* satellite, on the other hand, would yield all-sky SZE catalogue of very massive clusters; we find that the limits for $T_{\rm th} = 8$ keV clusters are nearly identical to those for $T_{\rm th} = 5$ keV systems.

In addition to probing its redshift evolution, the stacking approach is also useful for studying cosmic ray component in nearby low-mass clusters, and the dependence of X_p on cluster mass. Although individual clusters are not bright enough, cluster mass function predicts that there are a number of such low-mass clusters, which should help improve the *GLAST* sensitivity.

4.2 Extragalactic γ-ray background

Another avenue to constrain the universal average of X_p is to use the extragalactic γ-ray background (Sreekumar et al. 1998), because galaxy clusters would contribute to this background intensity to a certain extent. Their contribution is quantified as

$$I_\gamma = \int_0^\infty {\rm d}z \frac{{\rm d}^2 V}{{\rm d}z{\rm d}\Omega} \int_{M_{\rm th}}^\infty {\rm d}M \frac{{\rm d}n_{\rm h}}{{\rm d}M}(M,z) F_{X_p}(M,z), \quad (9)$$

which is quite similar to equation (6). Adopting the same models for ${\rm d}n_{\rm h}/{\rm d}M$ and F_{X_p} as in Section 4.1, and using $\alpha_p = 2.1, \beta = 0$, and $E_{\rm min} = 100$ MeV, we obtain

$$I_\gamma(>100\,{\rm MeV}) = 4 \times 10^{-7} X_p\ {\rm cm}^{-2}\ {\rm s}^{-1}\ {\rm sr}^{-1}. \quad (10)$$

Even with $X_p = 1$, this is much smaller than the measurement by *EGRET*: 10^{-5} cm^{-2} s^{-1} sr^{-1} (Sreekumar et al. 1998). This indicates that cosmic ray processes in galaxy clusters are very unlikely to contribute to the γ-ray background flux significantly, especially because it requires a very large value for X_p, which is already excluded by *EGRET* for some of nearby clusters. This result is consistent with the previous studies such as Colafrancesco & Blasi (1998). Hence, we conclude that the stacking method using resolved clusters introduced in Section 4.1 would provide much more stringent constraint on X_p than the approach using extragalactic γ-ray background.

However, we here mention a few possibilities that may render this approach more viable in the near future. Soon after launch, *GLAST* should start resolving many point sources (mainly blazars) that are now contributing to the background flux. Furthermore, using angular power spectrum of the γ-ray background map might enable to disentangle the origin (Ando & Komatsu 2006; Ando et al. 2007b). In addition, there is a claim that the measured γ-ray background flux is dominated by the Galactic foreground even at high latitude, and that there is no certain measurement of truly extragalactic component (Keshet, Waxman & Loeb 2004). In any of the cases above, the contribution from galaxy clusters might be found to be significantly smaller than the current observed flux, which would be useful to constrain X_p at higher redshifts.

5 X-RAY AND SZE CLUSTER MASS ESTIMATES

Future γ-ray observations of galaxy clusters will have the potential to place tight constraints on the non-thermal pressure provided by cosmic rays. These forthcoming γ-ray constraints will, in turn, provide important handle on systematic uncertainties in the X-ray and SZE cluster mass estimates based on the hydrostatic equilibrium of the ICM. The hydrostatic mass profile of a spherically symmetric cluster is given by

$$M(<r) = \frac{-r^2}{G\rho_{\rm g}} \left(\frac{{\rm d}P_{\rm th}}{{\rm d}r} + \frac{{\rm d}P_{\rm nt}}{{\rm d}r} \right), \quad (11)$$

where $M(<r)$ is the mass enclosed within radius r, $\rho_{\rm g}$ is the gas density, and $P_{\rm th}$ and $P_{\rm nt}$ are the thermal and the non-thermal contributions to the pressure. The thermal gas, measured directly with current X-ray and SZE observations, provides a significant fraction of the total pressure support. The contribution of the non-thermal pressure, on the other hand, is customarily assumed to be small ($\lesssim$10 per cent) outside of a cluster core (see e.g. Nagai, Kravtsov & Vikhlinin 2007b), and it is often ignored in the hydrostatic mass estimates based on X-ray and SZE data. The cosmic ray pressure, if present, is a potential source of systematic bias in the hydrostatic mass estimates of clusters (e.g. Enßlin et al. 1997; Rasia et al. 2006; Nagai et al. 2007a, and references therein).

In equation (11), a directly relevant quantity is pressure gradient rather than energy density X_p that we mainly discussed until this point. Currently, it is not possible to infer both pressure and its radial

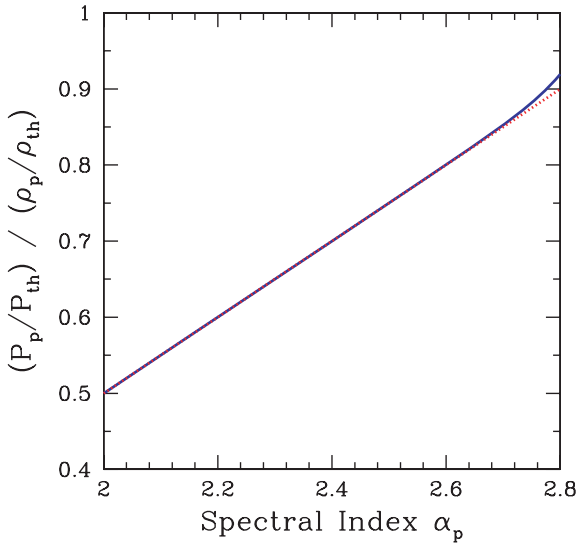

Figure 4. Relation between ratios of pressure ($Y_p = P_p/P_{th}$) and energy density ($X_p = \rho_p/\rho_{th}$) plotted as a function of spectral index α_p of cosmic rays (solid line). Dotted line is the linear fit $Y_p/X_p = 0.5\,(\alpha_p - 1)$.

profile, and here, we simply assume that the cosmic ray pressure profile is the same as that of thermal pressure. In this case, one needs to relate X_p to Y_p. If the cosmic rays are dominated by relativistic component, then equation of state would be $P_p = \rho_p/3$. On the other hand, for non-relativistic thermal gas, it is $P_{th} = 2\rho_{th}/3$. Thus, we expect $P_p/P_{th} = (1/2)(\rho_p/\rho_{th}) = X_p/2$. More precisely, we can obtain the equation of state for cosmic ray protons by numerically integrating the following expressions:

$$\rho_p = \int_0^\infty \mathrm{d}p\ f_p(p)\left(\sqrt{p^2 + m_p^2} - m_p\right), \tag{12}$$

$$P_p = \int_0^\infty \mathrm{d}p\ f_p(p)\frac{p^2}{3\sqrt{p^2 + m_p^2}}, \tag{13}$$

where $f_p(p) \propto p^{-\alpha_p}$ is the differential number density distribution. In Fig. 4, we show a correction factor between the pressure ratio Y_p and X_p, as a function of spectral index α_p. This relation is well fitted by a linear formula $Y_p/X_p = 0.5\,(\alpha_p - 1)$ as shown as a dotted line in Fig. 4; the deviation is only ∼0.3 per cent at $\alpha_p = 2.7$. As expected, for α_p close to 2, the ratio is about 0.5. Therefore, the expected sensitivity of *GLAST* for Y_p would be stronger than that for X_p given in Table 1 and as explicitly shown in Table 2. For $\alpha_p = 2.1$, *GLAST* sensitivities to Y_p based on the cluster stacking method are 5, 9 and 13 per cent at $0.05 < z < 0.10, 0.10 < z < 0.15$ and $0.15 < z < 0.25$, respectively. Note, however, that the conversion between Y_p and X_p depends on α_p, for which IACT measurements would be essential.

Observational constraints on $X_p = \langle\rho_p\rangle/\langle\rho_{th}\rangle$ is also sensitive to any non-negligible small-scale structure in the ICM. When gas clumps, it has density higher than the local average, $\langle\rho_{th}\rangle$. If it is not resolved and masked out, the local inhomogeneity in the ICM boosts γ-ray surface brightness by a factor of $C_\gamma \equiv \langle\rho_p\rho_{th}\rangle/\langle\rho_p\rangle\langle\rho_{th}\rangle$ and X-ray surface brightness by $C_X \equiv \langle\rho_{th}^2\rangle/\langle\rho_{th}\rangle^2$, while leaving SZE signal (which is linearly proportional to ρ_{th}) unaffected by clumpiness. A joint γ-ray + X-ray constraints on X_p based on a smooth model is generally biased by a factor C_γ/C_X, which could be greater or less than 1 depending on the relative size of C_γ and C_X.[3] A joint γ-ray + SZE constraint on X_p, on the other hand, is biased high by a factor C_γ. Recent cosmological simulations of clusters that include cosmic ray physics indicate jagged shape for the $X_p(r)$ profile, which implies a large clumping C_γ (Pfrommer et al. 2007). These simulations are potentially useful for estimating the values of C_γ, which would be important for interpretation of X_p in case of detection of cluster signals with upcoming γ-ray experiments. In absence of these constraints, observational constraints on X_p should be taken as an *upper limit*.

Recently, Mahdavi et al. (2007) performed a comparison between masses estimated with weak gravitational lensing and using the assumption of hydrostatic equilibrium, and showed that the latter masses are typically biased to be lower by 20 per cent. This result might indicate presence of the non-thermal pressure component. Upcoming γ-ray measurements of galaxy clusters could thus provide useful information on the origin of this mass discrepancy. Turbulence and magnetic fields are also potential sources of bias in X-ray and SZE cluster mass estimates. Recent numerical simulations of cluster formation indicate that subsonic motions of gas provide non-thermal pressure in clusters by about ∼10 per cent even in relaxed clusters (e.g. Rasia et al. 2006; Nagai et al. 2007a, and references therein). Most cluster atmospheres are also magnetized with typical field strengths of the order of a few μG out to Mpc radii (Carilli & Taylor 2002; Govoni & Feretti 2004), but this would only give negligible contribution to the total pressure support.

6 INVERSE COMPTON SCATTERING FROM NON-THERMAL ELECTRONS

6.1 Secondary electrons from pion decays

Until this point, we have neglected the contribution to γ-rays from relativistic electrons and positrons produced from decays of charged pions. Those charged pions are produced by the proton–proton collisions just as π^0s that decay into γ-rays. Thus, as long as the cosmic ray protons exist, there should also be relativistic $e^\pm$ component associated with them. GeV γ-rays would be produced by IC scattering of CMB photons due to such a 'secondary' leptonic component. In this subsection, we show the expected IC flux to compare it with the flux from π^0 decays, and argue that the former is indeed negligible, justifying our earlier treatment.

Unlike protons, leptons can cool quickly by synchrotron radiation and IC scattering. Energy distribution of these electrons (positrons) after cooling is obtained as a steady-state solution of the transport equation, which is

$$n_e(E_e, r) = \frac{1}{|\dot{E}_e(E_e, r)|}\int_{E_e}^\infty \mathrm{d}E'_e Q_e(E'_e, r), \tag{14}$$

where Q_e is the source function of injected electrons. For the energy-loss rate $\dot{E}_e$, the dominant interaction would be synchrotron radiation and IC scattering of CMB photons, i.e. $-\dot{E}_e \propto (U_B + U_{CMB})E_e^2$, where U_B and U_{CMB} are the energy densities of magnetic fields and CMB. If the injection spectrum is power law, $Q_e \propto E_e^{-\alpha_e}$,

[3] Current X-ray observations with superb spatial resolution and sensitivity are capable of detecting the prominent clumps that contribute significantly to the X-ray surface brightness. A comparison of recent X-ray and SZE measurements indicate that the X-ray clumping factor is very close to unity ($1 < C_X \lesssim 1.1$) in practice (LaRoque et al. 2006).

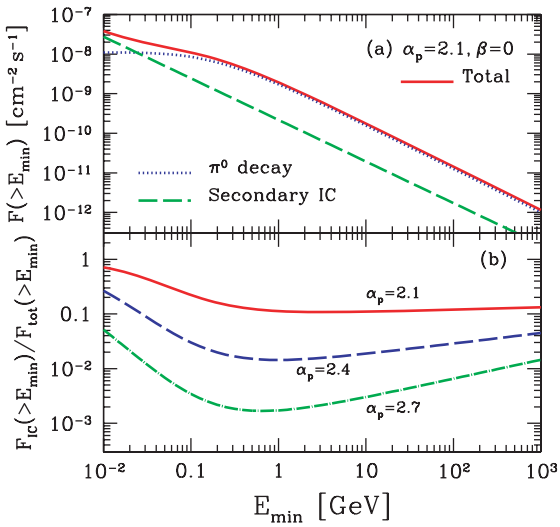

Figure 5. (a) Flux of γ-rays from π^0 decays with $X_p = 0.1$ (dotted), IC scattering due to secondary electrons (dashed) as a function of minimum energy E_{min}, for $\alpha_p = 2.1, \beta = 0$ and $B = 0$; total flux is indicated as a solid curve. (b) Fractional contribution of IC scattering to the total γ-ray flux, F_{IC}/F_{tot}, for $\alpha = 2.1$ (solid), 2.4 (dotted) and 2.7 (dashed).

then equation (14) states that the spectrum after cooling would be $n_e \propto E_e^{-\alpha_e-1}$, steeper by one power.

Once we know the electron distribution we can unambiguously compute the IC spectrum after scattering CMB photons. In addition, in the case of the secondary electrons, we can compute the source Q_e relatively well given the spectrum of cosmic ray protons. In Appendix B, we summarize fitting formula that we use, given by Dolag & Enßlin (2000) and Pfrommer & Enßlin (2004). Looking at equation (14), in order to get the electron distribution after cooling, we also need to know magnetic field strength B in the clusters that is relevant for synchrotron cooling. The estimates of B range ~0.1–10 μG (Clarke, Kronberg & Böhringer 2001; Fusco-Femiano et al. 2004; Rephaeli, Gruber & Arieli 2006), while the CMB energy density corresponds to equivalent field strength of $B_{CMB} = 3.24\ (1+z)^2$ μG. Thus, unless B is larger than or comparable to B_{CMB} everywhere in the cluster, the synchrotron cooling would not be significant, as the energy loss is proportional to $B^2 + B_{CMB}^2$. We here assume $B = 0$ to obtain the maximally allowed IC flux.

In Fig. 5(a), we show flux of IC γ-rays from secondary leptons, compared with direct γ-ray flux from π^0 decays, assuming $X_p = 0.1, \alpha_p = 2.1$ and $\beta = 0$. Fig. 5(b) shows the fractional contribution of the IC processes for various values of α_p. These figures show that even in the case of very week magnetic fields to reduce the electron energy losses, the IC processes give only subdominant flux in the GeV energy range relevant for *GLAST*. The fractional contribution of the IC emission to the total γ-ray flux, which is independent of X_p, is smaller than 20 per cent for $E_{min} = 100$ MeV and $\alpha = 2.1$. For a steeper proton spectrum ($\alpha > 2.1$), the fractional contribution becomes considerably smaller. Bremsstrahlung process due to the same electrons and positrons is even more suppressed (Blasi 2001). We thus conclude that the IC and bremsstrahlung γ-ray emission by secondary electrons are subdominant for the realistic range of parameters.

6.2 Primary electrons by shock acceleration

Whenever the shocks are generated, both ions and electrons are accelerated. Thus, one expects that the IC scattering off the CMB photons due to such primary electrons would also contribute to the GeV–TeV γ-ray flux to a certain extent (Loeb & Waxman 2000; Totani & Kitayama 2000; Waxman & Loeb 2000; Gabici & Blasi 2004). If this process dominates the π^0 decays in γ-ray energy band, then the constraints on X_p will be directly affected in case of detection. However, there are difficulties for this mechanism to work efficiently in many clusters.

As electrons lose their energies via radiation much more rapidly than protons, clusters would be bright with this mechanism during only a limited period after injection. For example, the radiative cooling time-scale for 10 GeV electrons is $\sim 10^8$ yr, which is much shorter than typical cluster age. By the same reason and also comparing the spatial intensity distribution, it is unlikely that synchrotron radiation from these primary electrons is responsible for the observed radio halo emissions (e.g. Blasi, Gabici & Brunetti 2007).

It might still be possible to overcome these difficulties if these electrons are continuously reaccelerated *in situ* through the second-order Fermi mechanism (Schlickeiser, Sievers & Thiemann 1987; Tribble 1993; Brunetti et al. 2001; Petrosian 2001). In this case, however, the spectrum of electrons has typically a cut-off at the Lorentz factor of $\lesssim 10^5$. This property, while explains spectrum of radio halo of Coma quite well (e.g. Reimer et al. 2004), would restrict the γ-ray flux in the GeV region due to the IC scattering and bremsstrahlung. In Fig. 1, we show the upper bound on these components in the case of Coma cluster as a dotted curve, taken from Reimer et al. (2004).

In consequence, as long as X_p is more than a few per cent, it would be unlikely that the primary electrons, whether they are directly injected or continuously reaccelerated, dominate the GeV γ-ray flux, at least in a large fraction of clusters. Even though primary electron component dominated the detected flux, the shape of γ-ray spectrum would be very different from π^0-decay component especially at low energies, which could be used as a diagnosis tool; this difference comes from the kinematics of π^0 decays. The *GLAST* energy band ranges down to ~20 MeV, which is especially important characteristic for that purpose. Moreover, observations in lower frequency bands such as radio, EUV and hard X-rays, are also important, because these emissions are understood as synchrotron radiation (for radio) and IC scattering (for EUV and hard X-rays) from non-thermal electrons.

6.3 Secondary leptons from ultrahigh-energy cosmic ray interactions

If protons are accelerated up to ultrahigh energies such as $\gtrsim 10^{18}$ eV in galaxy clusters, which may be plausible, these protons are able to produce $e^\pm$ pairs through the Bethe–Heitler process with CMB photons: $p\gamma_{CMB} \rightarrow pe^+e^-$. These high-energy $e^\pm$ pairs then IC scatter the CMB photons, producing GeV–TeV γ-rays (Aharonian 2002; Rordorf, Grasso & Dolag 2004; Inoue, Aharonian & Sugiyama 2005). In this case, the IC photons might dominate the π^0-decay γ-rays by many orders.

However, this mechanism depends significantly on the maximal acceleration energy of the protons. This is especially because the threshold energy of the Bethe–Heitler process is $\sim 10^{17}$–10^{18} eV, and it is unclear whether the magnetic fields are strong enough to confine these ultrahigh-energy protons for cluster ages. Even if the detected γ-rays are dominated by this mechanism, the spectrum would be quite different from the π^0-decay γ-rays and should be easily distinguishable (e.g. Inoue et al. 2005).

7 CONCLUSIONS

We investigated the capability of the current and future γ-ray detectors such as *GLAST* and IACTs for constraining the cosmic ray pressure contribution to the ICM.

(i) We showed that the upcoming *GLAST* measurements can be used to place stringent upper limits, 0.5–5 per cent, on the ratio of energy densities of the cosmic rays and thermal gas, X_p, for several nearby rich clusters. These limits are fairly insensitive to the assumed energy spectrum or the radial distribution of the cosmic ray protons for a reasonable range of models. We showed that IACT sensitivity to X_p is not as stringent as *GLAST*, but IACTs provide useful constraint on spectral index α_p, which in turn provide important constraints on the acceleration mechanisms of cosmic rays.

(ii) The stacking method offers a powerful technique to probe the cosmological evolution of X_p and Y_p with upcoming γ-ray observations. Using the latest cosmological models such as halo mass function and phenomenological relations that reproduce observed cluster properties, we showed that one-year all-sky survey with *GLAST* can place tight limits ($Y_p \lesssim 10$ per cent) on the evolution of mean cosmic ray pressure in clusters out to fairly high redshift ($z \lesssim 0.25$) by stacking signals from a large sample of known clusters. These constraints will correspond to an *upper* limit on the systematic uncertainties in the X-ray and SZE cluster mass estimates, due to non-thermal pressure provided by cosmic rays. In addition, since the halo merger rate is expected to increase with redshift (e.g. Gottlöber, Klypin & Kravtsov 2001) and such mergers can boost γ-ray signals (Pfrommer et al. 2007), the technique may provide insights into the relation between cosmic ray energy density and merger activities. The same approach will also enable one to probe cosmic ray populations in low-mass clusters.

(iii) We also evaluated the cluster contribution to the extragalactic γ-ray background using the latest models, and showed that even with $X_p = 1$, the contribution is only about 4 per cent of the measured flux. This indicates that this approach would not currently be very helpful to constrain X_p, but might become more useful in the future if a significant fraction of the background flux were resolved.

(iv) We showed that γ-rays due to IC scattering by both the primary and secondary electrons are likely subdominant relative to the γ-rays from π^0 decays in most of the clusters. We find that the fractional contribution of the IC flux by secondary electrons never exceeds $\sim$20 per cent for a reasonable range of parameters, independently of X_p. The contribution from the primary electrons will also be suppressed in many clusters, because either they cool very fast after injection or they cannot be accelerated up to very high energies in the reacceleration models. Moreover, multiwavelength observations in radio, EUV and hard X-ray wavebands will provide independent constraints on non-thermal electrons in clusters (e.g. Reimer et al. 2004), and such a consideration shows that the expected γ-ray flux from the primary electrons is indeed subdominant as long as $X_p > 0.02$ (Fig. 1). Even if these components were dominant in some clusters, the shape of γ-ray spectrum should provide diagnostics of the origin.

ACKNOWLEDGMENTS

We thank Christoph Pfrommer, Julie McEnery and Steven Ritz for useful comments. This work was supported by Sherman Fairchild Foundation.

REFERENCES

Aharonian F. A., 2002, MNRAS, 332, 215
Aharonian F. A., Hofmann W., Konopelko A. K., Völk H. J., 1997, Astropart. Phys., 6, 369
Albrecht A. et al., 2006, preprint (astro-ph/0609591)
Ando S., Komatsu E., 2006, Phys. Rev. D, 73, 023521
Ando S., Komatsu E., Narumoto T., Totani T., 2007a, MNRAS, 376, 1635
Ando S., Komatsu E., Narumoto T., Totani T., 2007b, Phys. Rev. D, 75, 063519
Atoyan A. M., Völk H. J., 2001, ApJ, 535, 45
Becker M. R. et al., 2007, ApJ, 669, 905
Berezinsky V. S., Blasi P., Ptuskin V. S., 1997, ApJ, 487, 529
Blasi P., 1999, ApJ, 525, 603
Blasi P., 2001, Astropart. Phys., 15, 223
Blasi P., Colafrancesco S., 1999, Astropart. Phys., 12, 169
Blasi P., Gabici S., Brunetti G., 2007, Int. J. Mod. Phys. A, 22, 681
Böhringer H. et al., 2001, A&A, 369, 826
Bradač M. et al., 2006, ApJ, 652, 937
Brunetti G., Setti G., Feretti L., Giovannini G., 2001, MNRAS, 320, 365
Brunetti G., Venturi T., Dallacasa D., Cassano R., Dolag K., Giancintucci S., Setti G., 2007, ApJ, 670, L5
Carilli C. L., Taylor G. B., 2002, ARA&A, 40, 319
Carlstrom J. E., Holder G. P., Reese E. D., 2002, ARA&A, 40, 643
Clarke T. E., Kronberg P. P., Böhringer H., 2001, ApJ, 547, L111
Colafrancesco S., Blasi P., 1998, Astropart. Phys., 9, 227
Dahle H., 2006, ApJ, 653, 954
Dolag K., Enßlin T. A., 2000, A&A, 362, 151
Enßlin T. A., Biermann P. L., Kronberg P. P., Wu X.-P., 1997, ApJ, 477, 560
Enßlin T. A., Lieu R., Biermann P. L., 1999, A&A, 344, 409
Evrard A. E., Metzler C. A., Navarro J. F., 1996, ApJ, 469, 494
Fusco-Femiano R., Orlandini M., Brunetti G., Feretti L., Giovannini G., Grandi P., Setti G., 2004, ApJ, 602, L73
Gabici S., Blasi P., 2003, ApJ, 583, 695
Gabici S., Blasi P., 2004, Astropart. Phys., 20, 579
Gottlöber S., Klypin A., Kravtsov A. V., 2001, ApJ, 546, 223
Govoni F., Feretti L., 2004, Int. J. Mod. Phys. D, 13, 1549
Haiman Z., Mohr J. J., Holder G. P., 2001, ApJ, 553, 545
Hu W., Kravtsov A. V., 2003, ApJ, 584, 702
Inoue S., Aharonian F. A., Sugiyama N., 2005, ApJ, 628, L9
Jenkins A., Frenk C. S., White S. D. M., Colberg J. M., Cole S., Evrard A. E., Couchman H. M. P., Yoshida N., 2001, MNRAS, 321, 372
Kawasaki W., Totani T., 2002, ApJ, 576, 679
Keshet U., Waxman E., Loeb A., Springel V., Hernquist L., 2003, ApJ, 585, 128
Keshet U., Waxman E., Loeb A., 2004, J. Cosmology Astropart. Phys., 04, 006
LaRoque S. J., Bonamente M., Carlstrom J. E., Joy M. K., Nagai D., Reese E. D., Dawson K. S., 2006, ApJ, 652, 917
Loeb A., Waxman E., 2000, Nat, 405, 156
Mahdavi A., Hoekstra H., Babul A., Henry J. P., 2007, preprint (arXiv:astro-ph/0710.4132)
Miniati F., 2002, MNRAS, 337, 199
Miniati F., 2003, MNRAS, 342, 1009
Miniati F., Ryu D., Kang H., Jones T. W., 2001, ApJ, 559, 59
Nagai D., Vikhlinin A., Kravtsov A. V., 2007a, ApJ, 655, 98
Nagai D., Kravtsov A. V., Vikhlinin A., 2007b, ApJ, 668, 1
O'Neill S. M., Tregillis I. L., Jones T. W., Ryu D., 2005, ApJ, 633, 717
Perkins J. S. et al., 2006, ApJ, 644, 148
Petrosian V., 2001, ApJ, 557, 560
Pfrommer C., Enßlin T. A., 2004, A&A, 413, 17
Pfrommer C., Enßlin T. A., Springel V., Jubelgas M., Dolag K., 2007, MNRAS, 378, 385
Pointecouteau E., Arnaud M., Pratt G. W., 2005, A&A, 435, 1
Rasia E. et al., 2006, MNRAS, 369, 2013
Reimer O., Pohl M., Sreekumar P., Mattox J. R., 2003, ApJ, 588, 155
Reimer A., Reimer O., Schlickeiser R., Iyudin A., 2004, A&A, 424, 773

Rephaeli Y., Gruber D., Arieli Y., 2006, ApJ, 649, 673
Rordorf C., Grasso D., Dolag K., 2004, Astropart. Phys., 22, 167
Rosati P., Borgani S., Norman C., 2002, ARA&A, 40, 539
Rybicki G. B., Lightman A. P., 1979, Radiative Processes in Astrophysics. Wiley-Interscience, New York
Sarazin C. L., 1986, Rev. Mod. Phys., 58, 1
Scharf C. A., Mukherjee R., 2002, ApJ, 580, 154
Schlickeiser R., Sievers A., Thiemann H., 1987, A&A, 182, 21
Smith G. P., Kneib J.-P., Smail I., Mazzotta P., Ebeling H., Czoske O., 2005, MNRAS, 359, 417
Sreekumar P. et al., 1998, ApJ, 494, 523
Totani T., Kitayama T., 2000, ApJ, 545, 572
Tribble P. C., 1993, MNRAS, 263, 31
Vikhlinin A., Kravtsov A., Forman W., Jones C., Markevitch M., Murray S. S., Van Speybroeck L., 2006, ApJ, 640, 691
Voit G. M., 2005, Rev. Mod. Phys., 77, 207
Völk H. J., Aharonian F. A., Breitschwerdt D., 1996, Space Sci. Rev., 75, 279
Waxman E., Loeb A., 2000, ApJ, 545, L11

APPENDIX A: γ-RAY EMISSIVITY FROM π^0 DECAYS

Equation (1) has a very clear structure including several relevant physics, ranging from cosmic ray distribution $n_{\rm p}(E_{\rm p},\ r)$ to π^0-production cross-section $\mathrm{d}\sigma_{\rm pp}/\mathrm{d}E_\pi$. This integral is no difficult, and indeed, Pfrommer & Enßlin (2004) gave a simple fitting form for that as follows:

$$q_\gamma(E,r) = \sigma_{\rm eff} c n_{\rm H}(r)\xi^{2-\alpha_\gamma}\frac{\tilde{n}_{\rm p}(r)}{\rm GeV}\frac{4}{3\alpha_\gamma}\left(\frac{m_\pi c^2}{\rm GeV}\right)^{-\alpha_\gamma} \times\left[\left(\frac{2E}{m_\pi c^2}\right)^{\delta_\gamma}+\left(\frac{2E}{m_\pi c^2}\right)^{-\delta_\gamma}\right]^{-\alpha_\gamma/\delta_\gamma}, \quad \text{(A1)}$$

where $\alpha_\gamma = \alpha_{\rm p}$ is the asymptotic spectral index of γ-rays that is the same as that for protons, $\delta_\gamma = 0.14\,\alpha_\gamma^{-1.6} + 0.44$, $\xi = 2$ is a constant pion multiplicity, and

$$\sigma_{\rm eff} = 32(0.96 + {\rm e}^{4.4-2.4\alpha_\gamma})\,{\rm mb} \quad \text{(A2)}$$

is the effective inelastic pp cross-section. This reproduces results of numerical computations of hadronic processes as well as accelerator data quite well.

As π^0s are produced by collisions between non-thermal cosmic ray ions and thermal ICM nucleons, γ-ray emissivity is proportional to the product of ICM density $n_{\rm H}$ and number density of cosmic rays. The latter quantity is effectively characterized by $\tilde{n}_{\rm p}$ and this is given by requiring that the fraction $X_{\rm p}$ of the thermal energy density $\rho_{\rm th}$ goes to cosmic ray energy density:

$$X_{\rm p}(r)\rho_{\rm th}(r) = \frac{\tilde{n}_{\rm p}(r) m_{\rm p} c^2}{2(\alpha_{\rm p}-1)}\left(\frac{m_{\rm p}c^2}{\rm GeV}\right)^{1-\alpha_{\rm p}} \times \mathcal{B}\left(\frac{\alpha_{\rm p}-2}{2},\frac{3-\alpha_{\rm p}}{2}\right), \quad \text{(A3)}$$

where $\mathcal{B}$ is the beta function, appearing when we integrate kinetic energy of each proton weighed by the momentum distribution function, and

$$\rho_{\rm th}(r) = \frac{3}{2}\left(1+\frac{1-3X_{\rm He}/4}{1-X_{\rm He}/2}\right) n_{\rm e}(r) k_{\rm B} T_{\rm e}(r), \quad \text{(A4)}$$

with $k_{\rm B}$ the Boltzmann constant, $X_{\rm He} = 0.24$ is the primordial mass fraction of ^{4}He, and the electron density $n_{\rm e}$ and temperature $T_{\rm e}$ are well measured with X-rays.

APPENDIX B: INVERSE COMPTON SCATTERING FROM SECONDARY ELECTRONS

Hadronic collisions also produce charged pions that eventually decay into electrons and positrons. These leptons, having relativistic energies, can up-scatter the CMB photons into GeV energies. Since the physics of IC scattering is well established (Rybicki & Lightman 1979) and pion production due to pp collisions are measured in laboratories, this process can be described with relatively small ambiguity.

Electron distribution function after radiative cooling is

$$n_{\rm e}(E_{\rm e},r) = \frac{\tilde{n}_{\rm e}(r)}{\rm GeV}\left(\frac{E_{\rm e}}{\rm GeV}\right)^{-\alpha_{\rm e}}, \quad \text{(B1)}$$

$$\tilde{n}_{\rm e}(r) = \frac{2^7\pi 16^{-(\alpha_{\rm e}-1)}}{\alpha_{\rm e}-2}\frac{\sigma_{\rm eff} m_{\rm e}^2 c^4}{\sigma_{\rm T}\,{\rm GeV}}\frac{n_{\rm H}(r)\tilde{n}_{\rm p}(r)}{B(r)^2+B_{\rm CMB}^2}, \quad \text{(B2)}$$

where $\alpha_{\rm e} = \alpha_{\rm p} + 1$, $\sigma_{\rm T}$ is the Thomson cross-section, and $B_{\rm CMB} = 3.24(1+z)^2\,\mu$G. Emissivity of IC scattered photons is given as

$$q_{\rm IC}(E,r) = \tilde{q}(r) f_{\rm IC}(\alpha_{\rm e})\left(\frac{m_{\rm e}c^2}{\rm GeV}\right)^{1-\alpha_{\rm e}} \times\left(\frac{E}{k_{\rm B}T_{\rm CMB}}\right)^{-(\alpha_\nu+1)},$$

$$\tilde{q}(r) = \frac{8\pi^2 r_{\rm e}^2 \tilde{n}_{\rm e}(r)(k_{\rm B}T_{\rm CMB})^2}{h^3c^2},$$

$$f_{\rm IC}(\alpha_{\rm e}) = \frac{2^{\alpha_{\rm e}+3}(\alpha_{\rm e}^2+4\alpha_{\rm e}+11)}{(\alpha_{\rm e}+3)^2(\alpha_{\rm e}+5)(\alpha_{\rm e}+1)} \times\Gamma\left(\frac{\alpha_{\rm e}+5}{2}\right)\zeta\left(\frac{\alpha_{\rm e}+5}{2}\right), \quad \text{(B3)}$$

where $\alpha_\nu = (\alpha_{\rm e}-1)/2$, $r_{\rm e}$ is the classical electron radius, $T_{\rm CMB} = 2.7$ K is the CMB temperature, Γ is the Γ-function and ζ is the Riemann ζ-function. For more detailed discussions, see Dolag & Enßlin (2000) and Pfrommer & Enßlin (2004).

APPENDIX C: *GLAST* SENSITIVITY FOR EXTENDED SOURCES

Flux sensitivity of *GLAST*–LAT to a point-like source is shown as a thick dashed line in Fig. 1. The sensitivity for an extended source is different; in this section, we derive it using a simple argument.

The dominant background is extragalactic γ-ray flux, and its intensity depends on photon energy as $I_{\rm bg} \propto E^{-2.1}$ (Sreekumar et al. 1998). At low energies where background photon count are larger than 1 ($N_{\rm bg} \gtrsim 1$), the flux sensitivity is determined by a criterion such as $N_{\rm lim} > \alpha\sqrt{N_{\rm bg}}$, where some number α sets significance of detection; hereafter use $\alpha = 5$. On the other hand, at higher energies where $N_{\rm bg} \lesssim 1$, then the detection simply relies upon photon count from a source.

Thus, for a source like galaxy clusters, there are up to four different energy regimes depending on the source extension. (i) At lowest energies where PSF (or pixel size) is larger than the source size (i.e. $\Omega_{\rm pix} > \Omega$), the source can be regarded as a point-like object. The other three regimes are for more energetic photons where source are extended ($\Omega > \Omega_{\rm pix}$); they are where background photon counts are (ii) larger than 1 from 1 pixel ($N_{\rm bg,pix} > 1$); (iii) smaller than 1 from 1 pixel but larger than 1 from the entire source region ($N_{\rm bg,pix} < 1, N_{\rm bg} > 1$); (iv) smaller than 1 from the entire source

region ($N_{\rm bg} < 1$). For the lowest energy region (i), the sensitivity is the same as that for point sources, and this corresponds to the regime below ~300 MeV in Fig. 1.

For the region (ii), the point-source flux sensitivity $F_{\rm lim,pix}$ are obtained by a criterion $N_{\rm lim,pix} = 5\sqrt{N_{\rm bg,pix}}$. These photon numbers are related to the flux and background intensity through $N_{\rm lim,pix} = F_{\rm lim,pix}AT$ and $N_{\rm bg,pix} = I_{\rm bg}AT\Omega_{\rm pix}$, where AT (effective area times exposure time) is the detector exposure. The point-source sensitivity is thus obtained by

$$F_{\rm lim,pix} = 5\sqrt{\frac{I_{\rm bg}\Omega_{\rm pix}}{AT}}. \tag{C1}$$

A similar argument can be applied for the flux sensitivity for an extended source $F_{\rm lim}$ and we obtain

$$F_{\rm lim} = 5\sqrt{\frac{I_{\rm bg}\Omega}{AT}} = F_{\rm lim,pix}\sqrt{\frac{\Omega}{\Omega_{\rm pix}}}. \tag{C2}$$

Thus the sensitivity becomes weaker by a factor of $\theta/\delta\theta_{\rm PSF}$, compared to that for a point-like source. This is the case for the region between 300 MeV and 2 GeV in Fig. 1.

When the photon energy becomes higher, the background count gets smaller. We then consider the region (iii). In this case, to obtain the point-source sensitivity, we use a criterion of five-photon detection: $F_{\rm lim,pix} = 5/AT$. As we have more background photons (than 1) from the entire source region, the extended-source flux sensitivity is the same as the first equality of equation (C2). Combining these two, we obtain

$$F_{\rm lim} = \sqrt{5F_{\rm lim,pix}I_{\rm bg}\Omega}, \tag{C3}$$

and this is for the region between 2 and 30 GeV in Fig. 1. At the highest regime (iv), the region above 30 GeV in Fig. 1, the cluster detection is totally relies on photon count and independent of background. Therefore, the sensitivity for an extended source is the same as that for a point-like source.

This paper has been typeset from a TEX/LATEX file prepared by the author.